ACS APPLIED MATERIALS & INTERFACES
Research Article
www.acsami.org

Evolution of Wurtzite ZnO Films on Cubic MgO (001) Substrates: A Structural, Optical, and Electronic Investigation of the Misfit Structures

Hua Zhou,[†] Hui-Qiong Wang,*[,†] Yaping Li,[†] Kongyi Li,[†] Junyong Kang,[†] Jin-Cheng Zheng,[†] Zheng Jiang,[‡] Yuying Huang,[‡] Lijun Wu,[§] Lihua Zhang,[∥] Kim Kisslinger,[∥] and Yimei Zhu[§]

[†]Key Laboratory of Semiconductors and Applications of Fujian Province, Department of Physics, Xiamen University, Xiamen 361005, P. R. China

[‡]Shanghai Synchrotron Radiation Facility, Shanghai Institute of Applied Physics, Chinese Academy of Sciences, Shanghai 201800, P. R. China

[§]Condensed Matter Physics and Materials Science Department, [∥]Center for Functional Nanomaterials, Brookhaven National Laboratory, Upton, New York 11973, United States

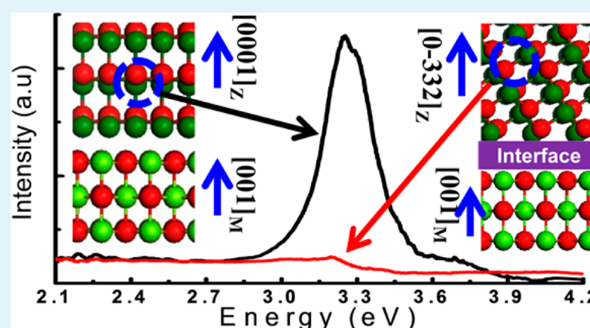

ABSTRACT: We investigated the interface between hexagonal ZnO films and cubic MgO (001) substrates, fabricated via molecular beam epitaxy. X-ray diffraction and (scanning) transmission electron microscopy revealed that growth follows the single [0001] direction when the temperature of the substrate is above 200 °C, while when the substrate temperature is below 150 °C, growth initially is along [0001] and then mainly changes to [0−332] variants beyond a thickness of ~10 nm. Interestingly, a double-domain feature with a rotational angle of 30° appears during growth along [0001] regardless of the temperature, experimentally demonstrating the theoretical predictions for the occurrence of double rotational domains in such a heteroepitaxy [Grundmann et al., *Phys. Rev. Lett.* 105, 146102 (2010)]. We also found that the optical properties of the ZnO film are influenced greatly by the mutation of growth directions, stimulated by the bond-length modulations, as we determined from X-ray absorption spectra at Zn K edge. These results also showed the evolution of the $4p_{xy}$ and $4p_z$ states in the conduction band with the rise in the temperature for growth. We consider that our findings may well promote the applications of ZnO in advanced optoelectronics for which its integration with other materials of different phases is desirable.

KEYWORDS: *ZnO, MgO, interface, transmission electron microscopy, X-ray absorption fine structure*

I. INTRODUCTION

ZnO, crystallizing in the wurtzite structure, is a typical semiconductor with a direct and wide band gap and a substantial free-exciton binding energy, whereas MgO is an insulator, exhibiting a simple rock-salt cubic structure. There are several good reasons for integrating ZnO and MgO. On the one hand, we can realize band-gap engineering on wurtzite ZnO through alloying it with cubic MgO; on the other hand, growing wurtzite ZnO on the MgO substrates might offer some guidelines for integrating wurtzite ZnO films with more complicated perovskite cubic substrates, for example, knowledge that is desirable for combining semiconductor-based "active" devices and perovskite-based "passive" ones. Already there are several reports[1−5] of ZnO thin films grown on MgO (001) substrates.

Interestingly, ZnO films can be grown along different crystalline directions on the same MgO (001) substrates under different conditions or methods of growth.[6−22] For instance, both oxygen partial pressure[14−18] and substrate temperature[19−22] influence growth orientations, although the underlying mechanisms of orientation are not yet clear. In this work, we detailed the atomic interfacial structure between the polar ZnO plane and the MgO (001) substrate employing high-resolution transmission electron microscopy (HRTEM) and scanning transmission electron microscopy (STEM) to follow the evolution of ZnO thin films via polycrystallization with multiple growth directions and single crystallization along the polar growth direction, which has been seldomly reported. In addition, we monitored the evolution of the electronic structure of the ZnO thin films through X-ray absorption fine structure (XAFS) spectra; there was no obvious evidence of the localization of the conduction band exhibited in amorphous ZnO films. The band structure changes of the ZnO films were also traced and are discussed herein.

Received: May 24, 2014
Accepted: July 23, 2014
Published: July 23, 2014

© 2014 American Chemical Society

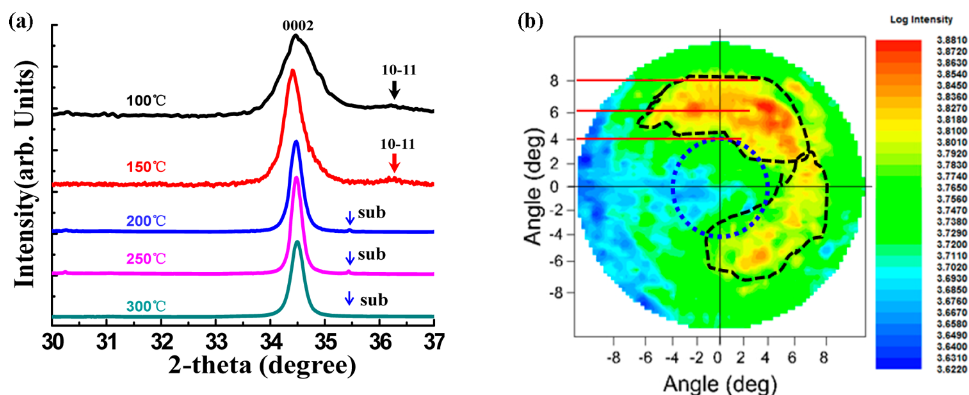

Figure 1. (a) XRD data for the grown ZnO thin films showing the highly [0001] *c*-axis-oriented texture for all temperatures, with additional 10−11 XRD peaks for films grown at 100 and 150 °C. The peak at 35.48° originates from the substrate. (b) The pole figure from the film grown at 150 °C with 2θ = 36.2°.

II. EXPERIMENTAL AND COMPUTATIONAL DETAILS

The ZnO films were grown on single-crystal MgO (001) substrates in an Omicron MBE system. Before inserting the substrates into the ultrahigh-vacuum chamber, they were cleaned ultrasonically first in acetone and subsequently in ethanol. The substrates' surfaces were then heated at 350 °C for an hour, in an oxygen plasma with a partial pressure of 5×10^{-5} mbar and a power of 250 W. The annealed MgO (001) surface showed streaky (1 × 1) reflection high-energy electron-diffraction (RHEED) patterns (not shown), similar to substrate whose surfaces were either treated at 420 °C for 60 min or at 250 and 350 °C each for 60 min.[19,23] ZnO films were deposited at a range of substrate temperatures with an oxygen partial pressure of 1×10^{-5} mbar and a plasma power of 250 W, while the evaporation rate of Zn (with a purity of 99.9999%) was maintained at 3 nm/min.

We characterized the textural orientation of the grown ZnO films using the Panalytical X'pert PRO X-ray diffraction facility. We used the peak positions for the substrates as references to calibrate the peak positions for each sample. The interface structure of ZnO (0001)/MgO (001) and the evolution of the ZnO thin film structures were examined using the JEOL2100F and JEM-ARM200CF for HRTEM and STEM, respectively, for which we employed the focused ion beam (FIB) in situ lift-out technique to prepare the TEM thin-film samples. The optical properties of the thin films were explored by transmission- and cathodoluminescence (CL)- spectra at room temperature. The electronic structures of the ZnO (0001) thin films were probed through X-ray absorption spectra (XAS), including X-ray absorption near-edge spectra (XANES) and extended X-ray absorption fine structure (EXAFS) collected on the BL14W1 beamline at Shanghai Synchrotron Radiation Facility (SSRF), Shanghai Institute of Applied Physics (SINAP), China. XANES, which indicates the features of condensed matter due to the photoabsorption cross-section for electronic transitions from an atomic core level to unoccupied final states, reflects information on the conduction band's structure, while the multiple-scattering-based EXAFS reveals the information about bond length and coordination number. The energy of the incident X-rays was selected through a Si (111) double-crystal monochromator with an incident angle of 45°. The XAS spectral data were collected in the fluorescence mode, utilizing a 32-element Ge solid-state detector with a digital X-ray processor system.

The band structure, density of states (DOS), and theoretical XANES spectra of ZnO were calculated using first-principles full-potential calculations based on density functional theory (DFT),[24] as implemented in WIEN2k package.[25] We employed the Perdew−Burke−Ernzerh of generalized gradient approximation (PBE-GGA)[26] to obtain the exchange-correlation function. The EXAFS analysis and fitting were performed using the IFEFFIT package.[27−29]

III. RESULTS AND DISCUSSION

A. Structural Evolution of (0001) ZnO/MgO (001).

Figure 1a shows the results from X-ray Diffraction (XRD) of a series of 60 min of growth of ZnO films on the MgO (001) surface, corresponding to substrate temperatures of 100, 150, 200, 250, and 300 °C. In the range from 200 to 300 °C, the strong intensity of the 0002 peak denotes the main (0001) orientation of the ZnO epilayer as we reported earlier,[19] notwithstanding a substrate temperature below 150 °C, while an additional peak of 10−11 appears, indicated by the arrow in Figure 1. Nevertheless, the apparently weaker intensity of the 10−11 peak compared to that of the 0002 peak does not necessarily indicate a smaller portion of tilted growth compared to the growth along the [0002] direction. One reason is that the structure factor (SF) also plays an important role in determining the peak's intensity $((SF0002/SF10-11)^2 = 60.5)$.[23] Furthermore, the direction of tilted growth actually is most likely along ~[0−332] rather than [0−111]* (the normal of the (0−111) plane) as determined from the STEM results for the 100 °C sample (see Figure 4b and the discussion later), whose corresponding azimuth deviates by about 3° from the [0−111]*. This result is similar to the observation of the XRD pole figure of {10−11} reflections (2θ = 36.2°; note that 10−11 and 0−111 overlap in XRD) from the 150 °C sample, as shown in Figure 1b. The pole figure shows that the growth direction of the (0−111) plane for the 150 °C sample tilts away by about 6° from the vertical direction of the MgO substrate, which is slightly larger (3°) than the tilted angle for the 100 °C sample because of the slight difference in growth temperature.

Furthermore, interestingly, the pole figure shows a non-symmetric pattern, as detailed by the dotted dark curved lines in Figure 1b, indicating the localization of the tilted growth direction. Therefore, we concluded that the 10−11 spot is off the Bragg position in XRD for both the 100 and 150 °C samples, resulting in its subsequent decrease in intensity as shown in Figure 1a; that is, from the macroscopic view of understanding the film's structure, the growth directions of the 100 °C—and 150 °C—samples deviate several degrees (ca. 3−8°) from the [0−111]* direction. To investigate the effect of substrate temperature on the structure of the ZnO films, we calculated the mean grain sizes of the five samples using the Scherrer equation:[23,30] $D = 0.94\lambda/(B \cos \theta)$, where D, λ, B, and θ, respectively, are the mean grain size, the X-ray wavelength (1.54 Å), the full-width-at-half-maximum (FWHM) of the peak in radians, and the Bragg diffraction angle, respectively. As

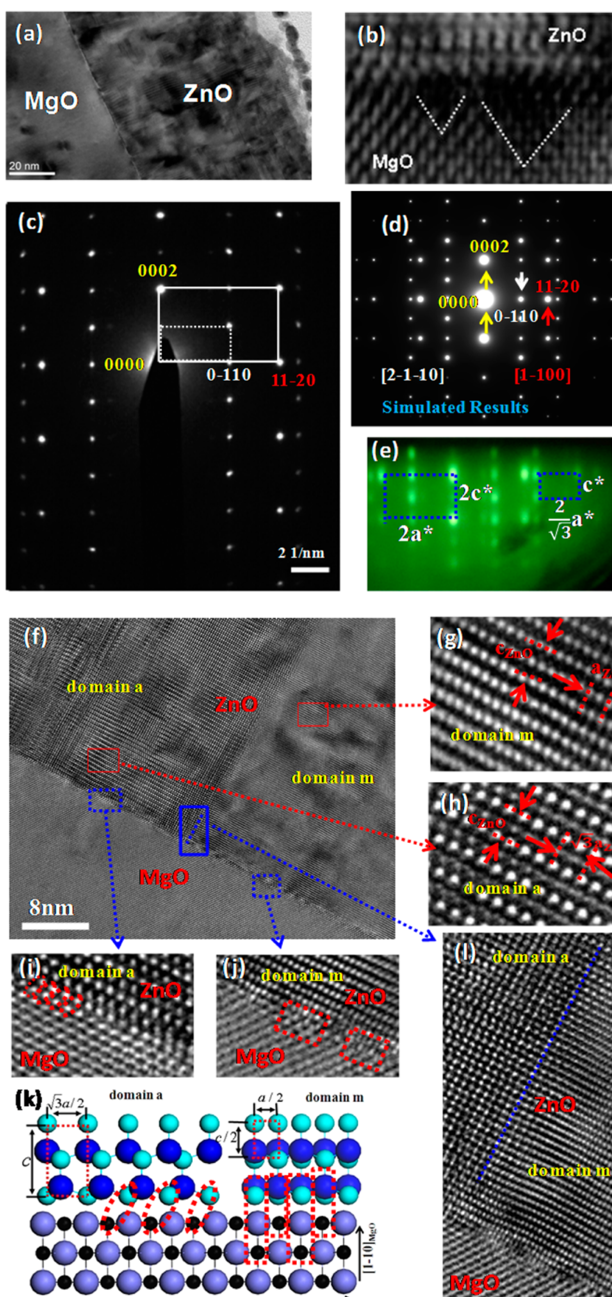

Figure 2. (a) Low-magnification TEM image of the ZnO/MgO interface from the 250 °C sample. (b) Further magnified image from the interface region, which shows "V-type" defects. (c) SAED patterns along the [110] MgO azimuth, showing diffraction spots from both the MgO substrate and the ZnO film with the double-domain film feature, consistent with our observations from the RHEED patterns and the calculated EDP image as shown in (d, e). (f) Higher resolution TEM image of the ZnO/MgO interface from the 250 °C sample, showing two kinds of domains. (g, h) Further magnified images of the rectangle areas (marked by solid red lines) from the two domain areas in (f) showing the lattice parameters a and c marked by red dotted lines equal to 3.26 and 5.24 Å, respectively. (i, j) The magnified images of the rectangle areas labeled by blue dotted lines, showing the positional relationship between Zn atoms and Mg atoms in the two kinds of domains labeled by the dotted circles and rectangle lines, respectively. (k) The corresponding atomic model of the interfacial structure from the side-view along the [110] MgO azimuth. (l) The interfacial structure between the two kinds of domains, as labeled by the blue dotted line.

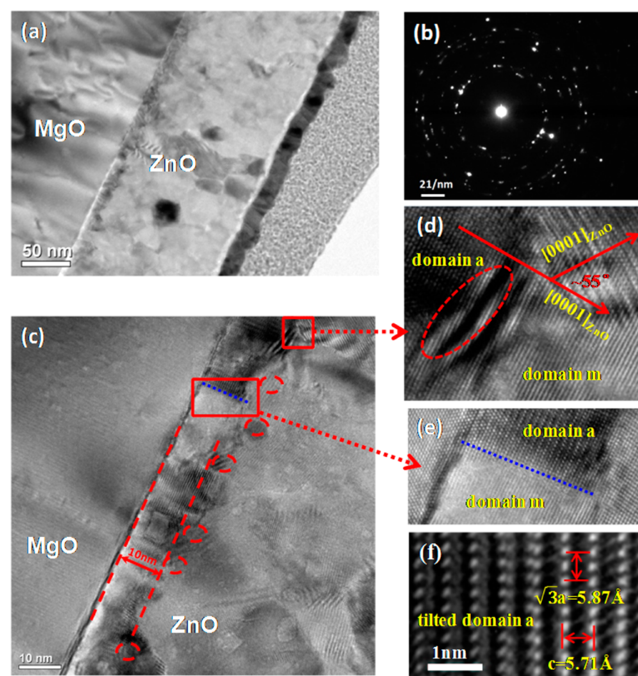

Figure 3. (a) Low-magnification TEM image of the ZnO/MgO interface from 100 °C sample. (b) The corresponding SAED pattern showing polycrystalline feature of the ZnO films. (c) High-resolution TEM image of the ZnO/MgO interface from the 100 °C sample showing that the initial growth along the [0001] azimuth is about 10 nm, as denoted by the red dotted lines, with the later multiple growth directions labeled by red dotted circles. (d, e) The magnified images of the rectangular areas from the ZnO film, which show the change of growth direction of the ZnO film from the [0001] azimuth to the [10−11] azimuth labeled by red arrows and its nanorod-like columnar growth labeled by the red dotted line. (f) Magnified images of HRTEM from a region grown along the [0−332] direction from the 100 °C sample, showing the lattice parameters of a and c = 3.39 and 5.57 Å, respectively, slightly larger than those for growth along the [0001] direction.

shown in Table I, the respective calculated mean grain sizes of the five film samples are approximately 11.1, 18.0, 30.9, 36.2, and 28.8 nm, indicating that the tendency of the grain sizes to change is first increasing and then decreasing. For substrate temperatures higher than 300 °C, the growth will turn to nonpolar direction, resulting in a decrement in grain size, as we previously reported.[19]

Figures 2 and 3 show the images from HRTEM captured along the [110] MgO azimuth from the ZnO films grown at 250 and 100 °C, respectively. The thickness of the 250 °C sample is about 80 nm, as determined from the low-magnification TEM image in Figure 2a. Figure 2c shows the corresponding selected-area electron-diffraction (SAED) pattern from the 250 °C sample; it reveals two sets of reciprocal lattices on the zone axis of MgO [110] (the SAED of the substrate is not shown), labeled as white solid- and white dashed-boxes, corresponding to the [2−1−10] domain (named the "m-domain") and the [1−100] domain (named the "a-domain"). The experimental electron-diffraction patterns agree with the simulated ones (Figure 2d). The corresponding RHEED pattern captured in situ immediately after growth indicates two sets of reciprocal lattices (labeled [2a*, 2c*] and [$(2/\sqrt{3})$a*, c*], respectively) for the side view of the epilayer, corresponding to the basic vectors of the reciprocal lattice for

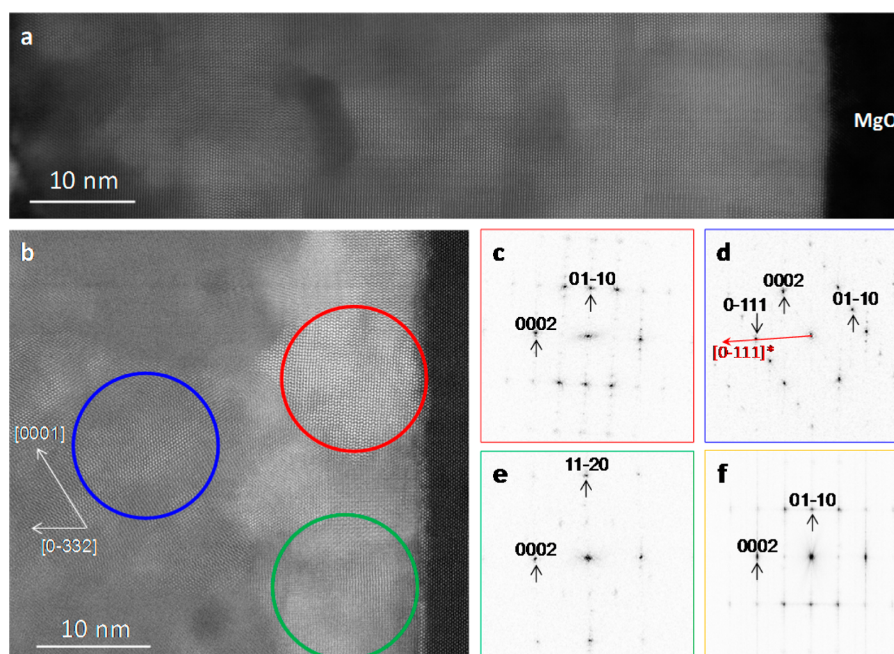

Figure 4. STEM images of the ZnO films grown at 250 °C (a) and 100 °C (b), showing the same interfacial structure between the films and the substrate, with different growth orientations beyond the interface region, as illustrated by the circles in (b). (c−e) Diffractograms from the (c) red-, (d) blue-, and (e) green-circled areas in (b). The red arrow in (d) points to the [0−111]* direction, which is the normal of the (0−111) plane, and deviates from the azimuth by about 3°. (f) The diffractogram from the film area in (a) for comparison.

Table I. XRD FWHM Values of the ZnO Films Grown at Different Temperatures and the Corresponding Grain Sizes

substrate temperature	100 °C	150 °C	200 °C	250 °C	300 °C
fwhm (deg)	0.776	0.475	0.281	0.239	0.296
grain size (nm)	11.1	18.0	30.9	36.2	28.8

the m-plane and the a-plane of ZnO, as illustrated in Figure 2e. The RHEED and SAED results are in excellent agreement. Also, the same RHEED patterns reappear at each 30° rotation of the sample, further demonstrating the coexistent domains rotating 30° from each other. In fact, for other samples of ZnO films grown along the [0001] direction, the RHEED patterns (not shown here) exhibit the same features, indicating that the interfacial structure of all the samples grown along the [0001] azimuth is the same.

Furthermore, the SAED pattern on the zone axis of MgO [110] in Figure 2c, and the fact that the aforementioned RHEED patterns (as shown in Figure 2e) always appear along the [110] direction of MgO, suggests that the registry relationship between the thin film and the substrate based on Figures 2 and 4 should be the following one:

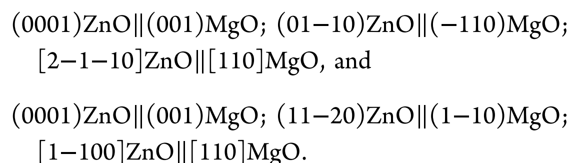
(0001)ZnO||(001)MgO; (01−10)ZnO||(−110)MgO; [2−1−10]ZnO||[110]MgO, and

(0001)ZnO||(001)MgO; (11−20)ZnO||(1−10)MgO; [1−100]ZnO||[110]MgO.

The observed RHEED patterns are similar to those of ZnO (0001) films grown on the MgO (001) substrates at a slightly different growth temperature, oxygen partial pressure, and plasma power,[19,31] highlighting the robustness of the structure of the double-domain (0001) surface for substrate temperatures below 300 °C. Hexagonal ZnO (0001) has a 6-fold symmetry, and cubic MgO (001) has a 4-fold one. The integration of both leads to two rotational domains in the epilayer due to the mismatch of rotational symmetry at the interface, as suggested by the following formula:[32]

$$N_{RD} = \frac{lcm(n, m)}{m} \quad (1,)$$

where N_{RD} is the number of rotational domains expected in the grown epilayer, n denotes the C_n rotational symmetry of the substrate crystal with rotation angles $\Phi_i = 2\pi/n$, m denotes the C_m rotational symmetry of the epilayer crystal with rotation angles $\Phi_j = 2\pi/m$, $lcm\ (n, m) = k/(i/n + j/m)$ is the least common multiple of n and m, where i, j, and k are integers. In our case, the cubic bulk MgO and hexagonal structure ZnO films have rotational symmetries of C_4 ($n = 4$) and C_6 ($m = 6$), respectively, and $lcm\ (4,6) = 12$. Therefore, $N_{RD} = 12/6 = 2$, that is, two rotational domains are expected in the hexagonal ZnO epilayer grown on the cubic MgO substrate, which is exactly what our results showed. Interestingly, a previous theoretical report[33] found that the boundary energy of a sample with a rotation angle of 30° is larger than one with a 32° rotation. Our observation of a stable rotation angle of 30° indicates the possibility that the interfacial energy between the thin films and the substrate for a rotation angle of 30°, with crystallographically equivalent interfaces in heteroepitaxy, is lower than that for a rotation of 32°, with enough energy to offset the increment of the boundary energy. Figure 2f shows a typical HRTEM image from the interface of the ZnO film and the MgO substrate and that of the rotational domains, indicating a modulation in structure across the interface. Figure 2g,h,i,j,l shows the corresponding magnified images labeled by rectangular areas from the ZnO film. Figure 2g,h, corresponding to the regions of the domain m and domain a, respectively, show their atomic structures. The values of structural parameters a and c of the ZnO thin film measured 3.26 and

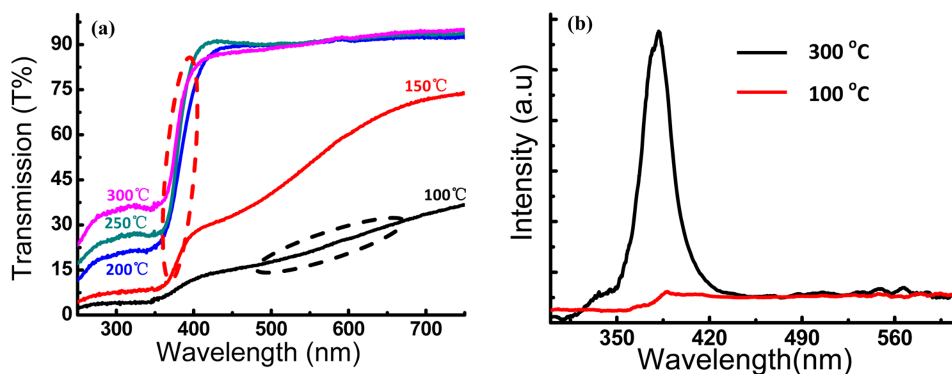

Figure 5. (a) The transmissivity of the films. The black dotted circle for the film grown at 100 °C indicates absorption of nearly the entire visible-light region. The red dotted circle corresponds to the film's band structure features. (b) The cathodoluminescence spectra (after smoothing) with an irradiation by a 6 keV electron beam from the 100 and 300 °C samples, respectively.

5.24 Å, respectively, that is, only about 0.3% and 0.6% larger than those of the ideal bulk ZnO (a = 3.25 Å and c = 5.21 Å), respectively, revealing a nearly fully relaxed thin film. However, the bonding configuration at the interface is more complex since the (0001) ZnO plane is polar, with Zn and O atoms stacking in alternative layers, while in the MgO (001) plane, both Mg and O atoms coexist with one dangling bond from each atom. Therefore, the interfacial structure cannot undergo a simple, direct transition from the MgO (001) surface to the ZnO (0001) polar surface, without any extra dangling bonds or twisted bands. Figure 2i,j, respectively, exhibits the interfacial structure (dotted red ovals) between domain a and the substrate and the interface (dotted red rectangles) between domain m and the substrate, clearly showing the atomic registry from the substrate (Mg) to the film (Zn). The corresponding atomic models of the interfacial structure are illustrated in Figure 2k. However, due to the mismatch between ZnO film and MgO substrate and the different surface atomic structure characteristics of the ZnO (0001) plane and MgO (001) plane, some dislocations and/or defects are expected at the interfaces. The HRTEM image in Figure 2b, for example, confirms the formation of the V-shaped defects near the interface (indicated by the white dashed lines), probably originating from the difficulty of bonding between the polar plane and surface of MgO (001) in the interface. Since the static barrier energy of each Mg atom in the (001) plane is only about 0.3 eV,[34] they could easily be detached from the surface, resulting in the formation of the defects when the substrate is heated during growth. Indeed, it has been reported[35] that point defects are found in the MgO (001) surface. Another interesting aspect to examine is the boundary interface between the two domains in the ZnO film. As shown in Figure 2l, at the domain interface, apparently there are stacking faults only along the c-axis. In the direction perpendicular to the c-axis, the atoms seem to be arranged smoothly across the domain interface.

Figure 3 shows cross-sectional TEM images from the 100 °C sample, also on the zone axis of MgO [110]. The thickness of the film in the sample grown at 100 °C is about 175 nm, as shown in the low-magnification TEM image (Figure 3a), indicating that the growth of ZnO at a substrate temperature below 150 °C is faster than that above 200 °C. However, such growth leads to polycrystalline ZnO film, as indicated by the SAED pattern in Figure 3b and also evident in the HRTEM image in Figure 3c. Figure 3d,e shows the corresponding magnified images of the rectangular regions marked by red lines in Figure 3c. They reveal the evolution of the growth direction: initially, growth is along ZnO [0001] with double domains (a and m), as is the case for growth at 250 °C; when the thickness of the thin film reaches about 10 nm, as marked by the red dotted lines, the growth direction mutates into multiple growth directions, as labeled by dotted red circles in Figure 3c. Further analysis on the high-resolution images in Figure 3d and others (not shown) from the 100 °C sample shows that the ZnO variants mainly are along the {0−332} group direction, slightly titled from that of the [10−11]*, whose corresponding XRD peaks appear in Figure 1. The TEM images also reveal that the portion of the thin film grown along the [10−11]* direction is much larger than that along the [0001] direction, in agreement with the previous XRD analysis. For initial growth along [0001], the boundary structure of the double domains indicated by the blue lines in Figure 3c,e, parallel to the growth direction, is similar to the growth at 250 °C. Furthermore, there appears additional boundary between domains a and m perpendicular to the growth direction, as labeled by the red arrow in Figure 3d.

Interestingly, at the initial growth stage, growth at 100 and 250 °C follow the same direction toward [0001] with the same double-domain feature. This is confirmed through the STEM images as depicted in Figure 4a,b, which, respectively, correspond to the 250 and 100 °C samples. These results imply that, at the initial stage, the substrate's structure plays the most important role in determining the film's structure that follows the rotational domain rule in heteroepitaxy predicted by Grundmann et al.,[32] regardless of the growth temperature. Beyond a film thickness of about 10 nm, growth at 250 °C remains the same as in the initial stage, while growth at 100 °C turns to other directions, as illustrated by the images of TEM in Figure 3c and STEM (indicated by circles) in Figure 4b. This could be due to the slower diffusion rate at lower temperatures, such that the localized growth orientation is influenced by stress. The reason why the mutation goes toward the [0−332] variants might be attributed to the angle of incidence of the beam flux; in fact, previous reports demonstrated that the growth direction of films can be thus controlled.[36−38] Furthermore, through analyzing other HRTEM images (e.g., Figure 3f), the values of lattice parameters (a = 3.27 Å, c = 5.23 Å), along [0001] were found to differ from those retracted along [0−332] directions (a = 3.39 Å, c = 5.57 Å) in some localized regions in the same thin film grown at 100 °C. The a and c values determined from the growth areas along [0001] are 0.6% and 0.4% larger than the ideal bulk values (a = 3.25 Å and c = 5.21 Å), respectively, and those determined from the

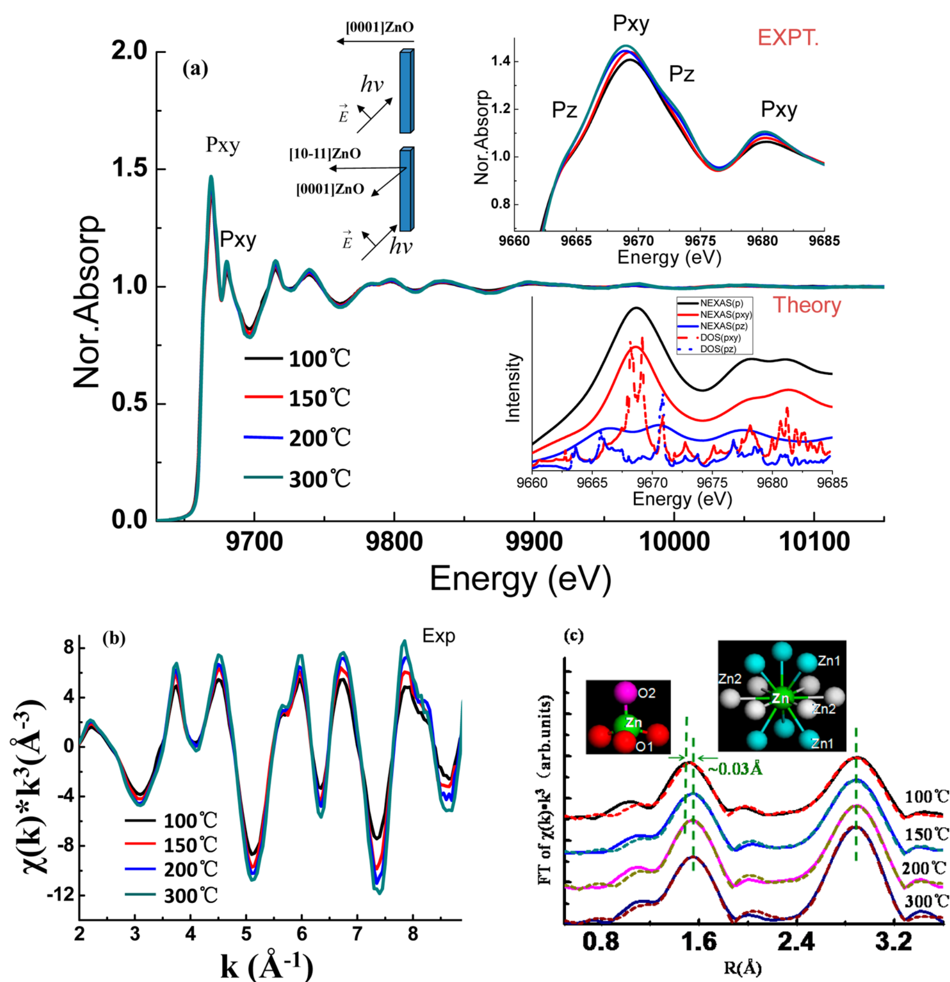

Figure 6. Zn K-edge X-ray absorption spectra of four ZnO films. (a) The measured full X-ray absorption spectra. The upper-left inset shows the direction of incident X-rays and the possible orientations of crystalline grains. The upper-right inset corresponds to the zoom-in NEXAS spectra within a narrower energy range (from 9660 to 9685 eV), with indication of Zn electronic orbital components, namely, p_{xy} and p_z. The NEXAS spectra for Zn K edge, including its p_{xy} and p_z components (i.e., NEXAS (p_{xy}) and NEXAS (p_z)), as well as p_{xy} and p_z projected density of states (i.e., DOS (p_{xy}) and DOS (p_z)), theoretically predicted also are shown in the lower-right inset. (b) $\chi(k)*k^3$ is represented as a function of k. The gradually enhancing amplitude reveals the gradually enlarging coordination number of the Zn atom during growth from 100 to 300 °C. (c) Magnitude of Fourier-transformed EXAFS using a Hanning window with a windowsill width of 0.5 Å. Data in the range of r = 1−3.8 Å were used for the fitting. The insets show the corresponding atomic geometric structures of the bonds of Zn−O1, Zn−O2, Zn−Zn1, and Zn−Zn2.

growth areas along [0−332] in some localized regions are 4.3% and 6.9% larger than the ideal bulk values, respectively. The discrepancy could have resulted from the occurrence of the tilted growth.

B. Optical and Electronic Properties of the ZnO Thin Films. To investigate the effect of substrate temperature on the optical properties of the ZnO thin films, we measured their transmissivities, with the transmissivity value of the MgO substrate set as 100%, and obtained their photoluminescence spectra as shown in Figure 5a,b, respectively. Undoubtedly, the transmissivity of visible light is reasonably high for ZnO films grown at higher substrate temperatures of 300, 250, and 200 °C and tends to decrease for films grown at lower substrate temperatures of 150 and 100 °C as shown by dark dashed circles. The evolution of the band structure also is indicated by the red dashed circles.

The possible reason for these results is that the better crystallization of films grown at higher substrate temperatures (above 200 °C) leads to a bulklike energy-band structure of ZnO, whereas films grown at lower substrate temperatures (below 150 °C) exhibit large disorders between grain boundaries, leading to different energy-band structure from that of bulk ZnO, such as a wider conduction band as reported before[39] as well as wider band tail; also, the occurrence of many defects increases the absorption of visible light. In fact, these conclusions were further confirmed by CL spectra with an irradiation of a 6 keV electron beam from the 100 and 300 °C samples, as shown in Figure 5b after smoothing. Comparing with the film grown at 100 °C with almost negligible band gap transition, the 300 °C sample performed a strong band-gap transition at the peak position of 381 nm (3.26 eV) with a FWHM of 32.4 nm (270 meV), revealing that the crystallization of film grown at 300 °C was better than that at 100 °C, in excellent agreement with the observation of transmission spectra.

The change of band structure is related to modulations in bond length that can be probed by extended X-ray absorption fine structure (EXAFS) spectra from the synchrotron-based equipment. Figure 6 shows the Zn-edge EXAFS results for ZnO films grown at 100, 150, 200, and 300 °C; it illustrates the evolution of electronic structure of the ZnO films from multiple growth directions (for growth at 100 and 150 °C) to a single

Table II

Zn−O1					
parameters[a]	model[b]	100 °C	150 °C	200 °C	300 °C
N	3.0	2.1(±0.2)	2.3(±0.2)	2.4(±0.2)	2.5(±0.2)
R (Å)	1.97	1.94(±0.01)	1.95(±0.01)	1.97(±0.01)	1.96(±0.01)
σ^2 (Å^2)		0.0043(±0.0016)	0.0038(±0.0012)	0.0031(±0.0012)	0.0036(±0.0014)
Zn−O2					
parameters[a]	model[b]	100 °C	150 °C	200 °C	300 °C
N	1.0	0.7(±0.1)	0.8(±0.1)	0.8(±0.1)	0.8(±0.1)
R (Å)	1.99	2. 10(±0.03)	2.08(±0.03)	1.98(±0.03)	1.98(±0.01)
σ^2 (Å^2)		0.0043(±0.0016)	0.0038(±0.0012)	0.0031(±0.0012)	0.0036(±0.0014)
Zn−Zn1					
parameters[a]	model[b]	100 °C	150 °C	200 °C	300 °C
N	6.0	5.1(±0.6)	5.4(±0.5)	5.8(±0.4)	5.9(±0.5)
R (Å)	3.21	3.18(±0.01)	3.17(±0.01)	3.19(±0.01)	3.20(±0.02)
σ^2 (Å^2)		0.0130(±0.0013)	0.0113(±0.0009)	0.0105(±0.0008)	0.0094(±0.0008)
Zn−Zn2					
parameters[a]	model[b]	100 °C	150 °C	200 °C	300 °C
N	6.0	5.1(±0.6)	5.4(±0.5)	5.8(±0.4)	5.9(±0.5)
R (Å)	3.25	3.27(±0.01)	3.28(±0.01)	3.23(±0.01)	3.24(±0.02)
σ^2 (Å^2)		0.0130(±0.0013)	0.0113(±0.0009)	0.0105(±0.0008)	0.0094(±0.0008)

[a]Coordination number (N), bond length R, and Debye−Waller factor (σ^2) of ZnO thin films grown at different substrate temperatures, determined through fitting the orientation-dependent EXAFS data measured at the Zn K edge. $S_0^{\,2}$ is fixed at 0.95 [refs 38 and 39] for all data fittings. [b]For the model calculation, we used a fully occupied wurtzite structure (space group: $P63m$) with a = 3.2495 Å and b = 5.2069 Å.

growth direction with two rotational domains (for growth at 200 and 300 °C). The EXAFS spectra were acquired in the fluorescence mode, which utilizes a 32-element Ge solid-state detector with a digital X-ray processor system. Incident X-ray energy was selected with a three-quarters tuned Si(111) double monochromator, and the incident angle of X-ray beam was 45°, as illustrated in the upper-left inset of Figure 6a. Although the grain sizes of the films differ (Table I), inducing a tremendous difference in the interfacial structures developed at low and high temperatures, the absorption peaks of all these film samples are well-aligned, except that the intensity of absorption peaks from the films grown at 100 and 150 °C is a little smaller than in those grown at 200 and 300 °C.

The results reveal no distinction of electronic structure at the bottom of the conduction band for the ZnO thin films even when the grain size becomes very small (∼10 nm). Previously, Cho et al.[40,41] reported that the structural disorders in amorphous ZnO thin films could induce the localization of the conduction band through limited hopping interactions and orbital hybridization between adjacent ions, as shown in XAS spectra. Such phenomena do not appear in Figure 6a, indicating that the localization of the conduction band may not result from the interfacial effect of grain boundaries. In fact, Oba et al.[42] demonstrated, using an ab initio plane-wave pseudopotential method, that the disorder bond and dangling bond between grain boundaries did not necessarily induce electronic states in the band gap due to the domination of the Zn 4s character at the bottom of the conduction band.

In Figure 6a, the magnified profiles of XANES, which can reflect the information on the unoccupied states of the hybridized states between O 2p and Zn 4sp orbits directly, as shown in the upper-right inset, exhibit mostly the $4p_{xy}$ empty states, because of the large ratio of $4p_{xy}$ states to $4p_z$ states. Besides, in ZnO films grown at higher temperatures of 200 and 300 °C, the $4p_z$ states appear slightly stronger than those grown at 100 and 150 °C. This could be due to the change in angle between the incident X-ray beam and the crystalline orientation. For the growth along [0001] at 200 and 300 °C, the angle between the incident X-ray beam and c-axis is about 45°; for the growth along the [0−332] direction, that direction changes to about 80°, which presents only $4p_{xy}$ empty states. The lower-right inset of Figure 6a, showing our calculated results of density of states (DOS) and theoretical XANES of ZnO using first-principles full-potential calculations based on density functional theory (DFT),[26] reveals the $4p_z$ states at the peak positions of 9666 and 9671 eV, demonstrating the weaker $4p_z$ features for ZnO films grown at 100 and 150 °C, compared to those films grown at 200 and 300 °C. This is due to the twisting of growth directions from [0001] to [0−332] in some regions of the former group. In fact, the absorption spectra indicate some partial growth with a tilted angle about 45° along the normal of the substrate, consistent with these discussions. Figure 6b shows the k^3-weighted $\chi(k)$ signal of EXAFS data, which reflects the scattering effects from other atoms around the given atom (a function of the photoelectron wave-vector k), and provides detailed information about the average immediate atomic environment of the given lattice (atom) site. The intensity of $\chi(k)$ increases with substrate temperature, revealing that the coordination number of Zn atoms also increases with substrate temperature. The EXAFS data were Fourier-transformed to r space and fitted to the theoretical EXAFS calculations using the IFEFFIT package,[27−29] as shown in Figure 6c. To minimize uncertainty, only the EXAFS data in the k range of 2.0−12.4 Å^{-1} were further analyzed. The fitting included single- and multiscattering paths, and the 95% polarization of the incident X-rays was taken into account in the data analysis.[43,44] The dotted lines in Figure 6c show the magnitudes of the Fourier-transformed EXAFS data from the ZnO films.

We note that the peaks are shifted by about 0.5 Å on the r axis from their actual bond lengths due to the phase shift of the backscattered photoelectrons. The data were fitted with a fully occupied model of a wurtzite structure, varying the parameters of bond length R, coordination number N, and the Debye−

Waller factor σ^2 (which includes thermal vibrations and static disorders and is set the same for Zn−O1 and Zn−O2, and the same for Zn−Zn1 and Zn−Zn2). Table II summarizes the fitting results. Combined with those in Table I, it is evident that the value of σ^2 declines as grain size increases, while the coordination number of the Zn ions increases gradually for bigger grain sizes, which is consistent with the $K^3 \cdot \chi(k)$ EXAFS data. The explanation again is related to the limited diffusion rate of adatoms for substrate temperatures below 150 °C, which hinders the expansion of the islands, resulting in many dangling bonds, thereby raising the disorder of thin films. Especially, the film grown at 100 °C shows a large degree of disorder (σ^2(Zn−Zn) ≈ 0.0130 at 100 °C, and yet σ^2(Zn−Zn) ≈ 0.0094 at 300 °C) with a much smaller coordination number of Zn atoms, close to those of amorphous ZnO films. In addition, the huge amounts of interfaces between grains, resulting from the mutation of growth orientation and the tilted epitaxy, as indicated by STEM images in Figure 4b, could also lead to an increment in the disorders and a reduced coordination number of the Zn atoms. In fact, many other HRTEM images (not shown) from the 100 °C sample strongly suggest that grain size and the mutation of the growth orientation produce grain boundaries and determine the disorder of the films, which, in turn, induce a change in the electronic and optical properties of the ZnO film. Accordingly, the transmissivity (10−30%) of the samples below 150 °C are far smaller than those (~90%) of the samples above 200 °C in the visible region, as shown in Figure 5a. According to the equivalency of atomic geometry (shown in the insets of Figure 6c), two sets of Zn−O bonds (i.e., Zn−O1 and Zn−O2) and two sets of Zn−Zn bonding (i.e., Zn−Zn1 and Zn−Zn2) were considered for fitting.

There is no obvious change in the values of *R*(Zn−Zn) for ZnO films grown at temperatures ranging from 100 to 300 °C, while the values of *R*(Zn−O2) from the 100 and 150 °C samples are 5% larger than those grown at 200 and 300 °C; the corresponding values of *R*(Zn−O1) shows a contrasting trend. However, the average volume of the ZnO unit cell does not show obvious change based on our calculations using the following equations:[45]

$$R(\mathrm{Zn} - \mathrm{Zn1}) = \sqrt{\frac{a^2}{3} + \frac{c^2}{4}} \quad (2,)$$

$$R(\mathrm{Zn} - \mathrm{Zn2}) = a \quad (3)$$

The fitting results do not correspond well with our observations from the HRTEM images that the structural parameters *a* and *c* from the 100 °C sample grown along the [0−332] direction are, in some localized regions, 4.3% and 6.9% larger than the corresponding theoretical values. This could be because the XAFS spectra reflect the overall structure of the films, including the information on the grain boundary, while the TEM images show the samples' localized structure. Also, because the statistical possibility of a Zn−O1 bond is about 3 times that of Zn−O2 bond, when the Zn−O1 bonds become shorter and the Zn−O2 bonds become longer, the overall result would be that the nearest Zn−O bond length becomes shorter, leading to the left shift of the peak position, as indicated by green dashed lines in Figure 6c. Because the change of the lattice length only occurs in some tilted growth region grown along the [0−332] azimuth at lower growth temperatures, including the grain boundary, according to the discussion of HRTEM, these results also imply that the σ-bonds (also called bilayer bonds)[45,46] become slightly shorter, and yet the π bonds (also called *c*-axis bonds)[46,47] of ZnO become slightly longer in that region. This modification of σ bond or π bond is not resolved from the XRD data, probably due to the method's limited resolution that detects the average structural information. As the p_{xy} and p_z states are very sensitive to bond length, extended or shortened bonds will result in the transfer of electronic states. That probably is another reason why we observed the narrower width of the near Zn−K edge absorption of ZnO films grown at 100 and 150 °C, compared to those grown at 200 and 300 °C, as illustrated in the lower-right inset of Figure 6a. Furthermore, these also may contribute to the change in band structure, which is sensitive to modulation of bond length. Consequently, the transmissivity of a film grown at 100 °C is only about one-fifth of those grown at 200 and 300 °C, as shown in Figure 5a. Thus, we concluded, as exemplified in the discussions above, that tilted epitaxy of ZnO thin films is disadvantageous for the film's quality.

Our work not only shows that the electronic structure of ZnO thin film is influenced by the grain size and growth direction but also suggests that controlling growth conditions can tailor the grain sizes and the growth direction of such films, and thus tailor their electronic structure. The investigation of grain-size dependence of ZnO nanostructures is of importance, as in recent decades, ZnO nanorods and nanowires have demonstrated particularly interesting properties and applications. For example, they can be used to tune electronic and optoelectronic devices that involve UV-lasing action.[48,49] Knowledge of the electronic structure of nanorods or thin film grains is crucial to understanding the basic physics for these applications.

IV. CONCLUSIONS

In summary, we report the growth of wurtzite ZnO (0001) films on cubic MgO (001) substrates by molecular beam epitaxy. For substrate temperatures below 150 °C, the growth orientation of ZnO thin films exhibits a mutation from single polar-growth direction to multiple growth directions, while for substrate temperatures from 200 to 300 °C, orientation is only along [0001], based on XRD- and (S)TEM-analyses. For the growth along [0001], inevitably there appear to be two preferred in-plane rotational domains with a twist angle of 30°, and the interface relationship is as follows: (0001)ZnO ∥ (001)MgO; (01−10)ZnO ∥ (−110)MgO; [2−1−10]ZnO ∥ [110]MgO and (0001)ZnO ∥ (001)MgO; (11−20)ZnO ∥ (1−10)MgO; [1−100]ZnO ∥ [110]MgO. Furthermore, V-type defects were identified in the interface area resulting from the small barrier energy for Mg atoms in the (001) plane. For explaining the mutation orientation of the films, we consider that due to the large ratio of surface-to-bulk, there appears to be a higher degree of disorder and a smaller coordination number compared to the growth orientation only along [0001]. Besides, for some localized region of thin film grown along the [0−332] azimuth at the lower growth temperature of 100 °C, the lattice parameters of *a* and *c* are determined to be 3.39 and 5.57 Å, which, respectively, are 4.3% and 6.9% larger than theoretical values. These phenomena also lead to a dramatic change of band structure, as illustrated by the transmissivity and cathodoluminescence measurements. However, the XAS spectra reveal that the large disorder of the ZnO films between grain boundaries does not necessarily lead to the distinctive electronic states at the bottom of the conduction band, as observed in amorphous ZnO films; instead, the disorder results

in slightly shorter σ bonds and yet slightly longer π bonds, causing a dramatic change of the band structure.

AUTHOR INFORMATION

Corresponding Author

*E-mail: hqwang@xmu.edu.cn.

Notes

The authors declare no competing financial interest.

ACKNOWLEDGMENTS

This work was supported by Natural Science Foundation of China (Grant Nos. 11204253, U1232110, U1332105, 61227009, and 91321102), the Specialized Research Fund for the Doctoral Program of Higher Education (Grant No. 20120121110021), the Fundamental Research Funds for Central Universities (Grant Nos. 2012121012, 2013SH001), and the National High-Tech R&D Program of China (863 Program, No. 2013AA050901). Research carried out (in part) at Condensed Matter Physics and Materials Science Department and the Center for Functional Nanomaterials, Brookhaven National Laboratory, was supported by the U.S. Department of Energy, Office of Basic Energy Sciences, under Contract No. DE-AC02-98CH10886.

REFERENCES

(1) Matsunami, N.; Itoh, M.; Takai, Y.; Tazawa, M.; Sataka, M. Ion Beam Modification of ZnO Thin Films on MgO. *Nucl. Instrum. Methods Phys. Res., Sect. B* **2003**, *206*, 282−286.

(2) Nistor, L. C.; Ghica, C.; Matei, D.; Dinescu, G.; Dinescu, M.; Tendeloo, G. V. Growth and Characterization of a-axis Textured ZnO Thin Films. *J. Cryst. Growth* **2005**, *277*, 26−31.

(3) Deng, R.; Yao, B.; Li, Y. F.; Li, B. H.; Zhang, Z. Z.; Zhao, H. F.; Zhang, J. Y.; Zhao, D. X.; Shen, D. Z.; Fan, X. W.; Yang, L. L.; Zhao, Q. X. Surface Morphology, Structural, and Optical Properties of Polar and Non-Polar ZnO Thin Films: A Comparative Study. *J. Cryst. Growth* **2009**, *311*, 4398−4401.

(4) Seo, S. H.; Kang, H. C. The Crossover of Preferred Orientation in Heteroepitaxial ZnO/MgO(0 0 1) Films. *J. Cryst. Growth* **2011**, *326*, 166−170.

(5) Lu, C.-Y. J.; Chang, L.; Ploog, K. H.; Chou, M. M. C. Epitaxial Growth of Nonpolar ZnO on MgO (1 0 0) Substrate by Molecular Beam Epitaxy. *J. Cryst. Growth* **2013**, *378*, 172−176.

(6) Nistor, M.; Mandache, N. B.; Perrière, J.; Hebert, C.; Gherendi, F.; Seiler, W. Growth, Structural and Electrical Properties of Polar ZnO Thin Films on MgO (100) Substrates. *Thin Solid Films* **2011**, *519*, 3959−3964.

(7) Scarisoreanu, N.; Matei, D. G.; Dinescu, G.; Epurescu, G.; Ghica, C.; Nistor, L. C.; Dinescu, M. Properties of ZnO Thin Films Prepared by Radio-Frequency Plasma Beam Assisted Laser Ablation. *Appl. Surf. Sci.* **2005**, *247*, 518−525.

(8) Huang, K.; Tang, Z.; Zhang, L.; Yu, J.; Lv, J.; Liu, X.; Liu, F. Preparation and Characterization of Mg-Doped ZnO Thin Films by Sol−Gel Method. *Appl. Surf. Sci.* **2012**, *258*, 3710−3713.

(9) Zamfirescu, M.; Dinescu, A.; Danila, M.; Socol, G.; Radu, C. The Role of the Substrate Material Type in Formation of Laser Induced Periodical Surface Structures on ZnO Thin Films. *Appl. Surf. Sci.* **2012**, *258*, 9385−9388.

(10) Besleaga, C.; Stan, G. E.; Galca, A. C.; Ion, L.; Antohe, S. Double Layer Structure of ZnO Thin Films Deposited by RF-magnetron Sputtering on Glass Substrate. *Appl. Surf. Sci.* **2012**, *258*, 8819−8824.

(11) Benetti, M.; Cannatá, D.; Pietrantonio, F. D.; Verona, E.; Verardi, P.; Scarisoreanu, N.; Matei, D.; Dinescu, G.; Moldovan, A.; Dinescu, M. Structural and Piezoelectric Properties of Pulsed Laser Deposited ZnO Thin Films. *Superlattices Microstruct.* **2006**, *39*, 366−375.

(12) Cagin, E.; Yang, J.; Wang, W.; Phillips, J. D.; Hong, S. K.; Lee, J. W.; Lee, J. Y. Growth and Structural Properties of m-plane ZnO on MgO (001) by Molecular Beam Epitaxy. *Appl. Phys. Lett.* **2008**, *92*, 233505.

(13) Cui, Y.; Du, G.; Zhang, Y.; Zhu, H.; Zhang, B. Growth of ZnO (0 0 2) and ZnO (1 0 0) Films on GaAs Substrates by MOCVD. *J. Cryst. Growth* **2005**, *282*, 389−393.

(14) Fujimura, N.; Nishihara, T.; Goto, S.; Xu, J.; Ito, T. Control of Preferred Orientation for ZnO_x Films: Control of Self-texture. *J. Cryst. Growth* **1993**, *130*, 269−279.

(15) Yanagitani, T.; Kiuchi, M. Control of In-plane and Out-of-plane Texture in Shear Mode Piezoelectric ZnO Films by Ion-beam Irradiation. *J. Appl. Phys.* **2007**, *102*, 044115.

(16) Hada, T.; Wasa, K.; Hayakawa, S. Structures and Electrical Properties of Zinc Oxide Films Prepared by Low Pressure Sputtering System. *Thin Solid Films* **1971**, *7*, 135−145.

(17) Sharma, P.; Sreenivas, K.; Rao, K. V. Analysis of Ultraviolet Photoconductivity in ZnO Films Prepared by Unbalanced Magnetron Sputtering. *J. Appl. Phys.* **2003**, *93*, 3963−3970.

(18) Lu, J.; Ye, Z.; Huang, J.; Wang, L.; Zhao, B. Synthesis and Properties of ZnO Films with (1 0 0) Orientation by SS-CVD. *Appl. Surf. Sci.* **2003**, *207*, 295−299.

(19) Zhou, H.; Wang, H.-Q.; Liao, X.-X.; Zhang, Y.-F.; Zheng, J.-C.; Wang, J.-O.; Muhemmed, E.; Qian, H.-J.; Ibahim, K.; Chen, X. H.; Zhan, H. H.; Kang, J. Y. Tailoring of Polar and Nonpolar ZnO Planes on MgO (001) Substrates through Molecular Beam Epitaxy. *Nanoscale Res. Lett.* **2012**, *7*, 184.

(20) Pung, S. Y.; Choy, K.-L.; Hou, X.; Shan, C. Preferential Growth of ZnO Thin Films by the Atomic Layer Deposition Technique. *Nanotechnology* **2008**, *19*, 435609.

(21) Li, X. H.; Huang, A. P.; Zhu, M. K.; Xu, Sh. L.; Chen, J.; Wang, H.; Wang, B.; Yan, H. Influence of Substrate Temperature on the Orientation and Optical Properties of Sputtered ZnO Films. *Mater. Lett.* **2003**, *57*, 4655−4659.

(22) Nicolay, S.; Fay, S.; Ballif, C. Growth Model of MOCVD Polycrystalline ZnO. *Cryst. Growth Des.* **2009**, *9*, 4957−4962.

(23) Zhou, H.; Wang, H.-Q.; Wu, L.; Zhang, L.; Kisslinger, K.; Zhu, Y.; Chen, X. H.; Zhan, H. H.; Kang, J. Y. Wurtzite ZnO (001) Films Grown on Cubic MgO (001) with Bulk-Like Optoelectronic Properties. *Appl. Phys. Lett.* **2011**, *99*, 141917.

(24) Kohn, W.; Sham, L. J. Self-Consistent Equations Including Exchange and Correlation Effects. *Phys. Rev.* **1965**, *140*, 1133−1138.

(25) Blaha, P.; Schwarz, K.; Madsen, G. K. H.; Kvasnicka, D.; Luitz, J. *WIEN2k, An Augmented Plane Wave Plus Local Orbitals Program for Calculating Crystal Properties;* University of Technology: Vienna, Austria, 2001; pp 7−28.

(26) Perdew, J. P.; Burke, K.; Ernzerhof, M. Generalized Gradient Approximation Made Simple. *Phys. Rev. Lett.* **1996**, *77*, 3865−3868.

(27) Newville, M. IFEFFIT: Interactive XAFS Analysis and FEFF Fitting. *J. Synchrotron Radiat.* **2001**, *8*, 322−324.

(28) Ravel, B.; Newville, M. ATHENA, ARTEMIS, HEPHAESTUS: Data Analysis for X-ray Absorption Spectroscopy Using IFEFFIT. *J. Synchrotron Radiat.* **2005**, *12*, 537−541.

(29) Ravel, B. ATOMS: Crystallography for the X-ray Absorption Spectroscopist. *J. Synchrotron Radiat.* **2001**, *8*, 314−316.

(30) Li, B. S.; Liu, Y. C.; Chu, Z. S.; Shen, D. Z.; Lu, Y. M.; Zhang, J. Y.; Fan, X. W. High Quality ZnO Thin Films Grown. *J. Appl. Phys.* **2002**, *91*, 501−505.

(31) Park, S.-H.; Seo, S.-Y.; Kim, S.-H.; Han, S.-W. Surface Roughness and Strain Effects on ZnO Nanorod Growth. *Appl. Phys. Lett.* **2006**, *88*, 251903.

(32) Grundmann, M.; Böntgen, T.; Lorenz, M. Occurrence of Rotation Domains in Heteroepitaxy. *Phys. Rev. Lett.* **2010**, *105*, 146102.

(33) Chen, J.; Ruterana, P.; Nouet, G. Structural Units and Low-Energy Configurations of [0001] Tilt Grain Boundaries in GaN. *Phys. Rev. B* **2003**, *67*, 205210.

(34) Geneste, G.; Morillo, J.; Finocchi, F. Adsorption and Diffusion of MgO and O_2 on the MgO(001) Flat Surface. *J. Chem. Phys.* **2005**, *122*, 174707.
(35) Barth, C.; Henry, C. R. Atomic Resolution Imaging of the (001) Surface of UHV Cleaved MgO by Dynamic Scanning Force Microscopy. *Phys. Rev. Lett.* **2003**, *91*, 196102.
(36) Lintymer, J.; Martin, N.; Chappe, J.-M.; Takadoum, J. Glancing Angle Deposition to Control Microstructure and Roughness of Chromium Thin Films. *Wear* **2008**, *264*, 444−449.
(37) Zhang, Z.; Fan, X.; Lin, M.; Guo, D.; Chai, G.; Xue, D. Optimized Soft Magnetic Properties and High-Frequency Characteristics of Obliquely Deposited Co−Zr Thin Films. *J. Phys. D: Appl. Phys.* **2010**, *43*, 085002.
(38) Phuoc, N. N.; Xu, F.; Ong, C. K. Tuning Magnetization Dynamic Properties of Fe−SiO_2 Multilayers by Oblique Deposition. *J. Appl. Phys.* **2009**, *105*, 113926.
(39) Thouless, D. J. Electrons in Disordered Systems and the Theory of Localization. *Phys. Rep.* **1974**, *13*, 93−142.
(40) C, D.-Y.; Kim, J. H.; Hwang, C. S. Electron Hopping Interactions in Amorphous ZnO Films Probed by X-ray Absorption Near Edge Structure Analysis. *Appl. Phys. Lett.* **2011**, *98*, 222108.
(41) Cho, D.-Y.; Kim, J. H.; Na, K. D.; Song, J.; Hwang, C. S.; Park, B.-G.; Kim, J.-Y.; Min, C.-H.; Oh, S.-J. Spectroscopic Evidence for Limited Carrier Hopping Interaction in Amorphous ZnO Thin Film. *Appl. Phys. Lett.* **2009**, *95*, 261903.
(42) Oba, F.; Nishitani, S. R.; Adachi, H. I.; Tanaka, M. K.; Tannaka, S. Ab Initio Study of Symmetric Tilt Boundaries in ZnO. *Phys. Rev. B* **2001**, *63*, 045410.
(43) Han, S.-W.; Yoo, H.-J.; An, S. J.; Yoo, J.; Yi, G.-C. Orientation-Dependent X-ray Absorption Fine Structure of ZnO Nanorods. *Appl. Phys. Lett.* **2005**, *86*, 021917.
(44) Yu, H. J.; Jeong, E. S.; Park, S. H.; Seo, S. Y.; Kim, S. H.; Han, S. W. Orientation-Dependent Structural Properties and Growth Mechanism of ZnO Nanorods. *AIP Conf. Proc.* **2007**, *879*, 1865−1870.
(45) Haug, J.; Chassé; Dubiel, M.; Eisenschmidt, Ch.; Khalid, M.; Esquinazi, P. Characterzation of Lattice Defects by X-ray Absorption Spectroscopy at the Zn K-Edge in Ferromagnetic, Pure ZnO Films. *J. Appl. Phys. (Melville, NY, U. S.)* **2011**, *110*, 063507.
(46) Lawniczak-Jablonska, K.; Suski, T.; Gorczyca, I.; Christensen, N. E.; Attenkofer, K. E.; Perera, R. C. C.; Gullikson, E. M.; Underwood, J. H.; Ederer, D. L.; Lilienthal-Weber, Z. Electronic States in Valence and Conduction Bands of Group-III Nitrides: Experiment and Theory. *Phys. Rev. B* **2000**, *61*, 16623−16632.
(47) Chiou, J. W.; Mookerjee, S.; Rao, K. V. R.; Jan, J. C.; Tsai, H. M.; Asokan, K.; Pong, W. F.; Chien, F. Z.; Tsai, M.-H.; Chang, Y. K.; Chen, Y. Y.; Lee, J. F.; Lee, C. C.; Chi, G. C. Angle-Dependent X-ray Absorption Spectroscopy Study of Zn-Doped GaN. *Appl. Phys. Lett.* **2002**, *81*, 3389−3391.
(48) Huang, M. H.; Mao, S.; Feick, H.; Yan, H.; Wu, Y.; Kind, H.; Weber, E.; Russo, R.; Yang, P. Room-Temperature Ultraviolet Nanowire Nanolasers. *Science* **2001**, *292*, 1897−1899.
(49) Chen, R.; Ye, Q.-L.; He, T.; Ta, V. D.; Ying, Y.; Tay, Y. Y.; Wu, T.; Sun, H. Exciton Localization and Optical Properties Improvement in Nanocrystal-embedded ZnO Core-Shell Nanowires. *Nano Lett.* **2013**, *13*, 734−739.